RSC Advances

PAPER

View Article Online
View Journal | View Issue

Cite this: *RSC Adv.*, 2020, **10**, 35226

Fabrication of polyvinyl alcohol hydrogels with excellent shape memory and ultraviolet-shielding behavior *via* the introduction of tea polyphenols†

Xike Xiong,[a] Jun Sun,[a] Di Hu,[a] Chao Xiao,[a] Jianjun Wang,[a] Qiqi Zhuo,*[b] Chuanxiang Qin *[a] and Lixing Dai *[a]

Shape-memory hydrogels are expected to be used not only in an ordinary environment, but also in some special environments, such as under ultraviolet (UV) irradiation. Developing novel shape-memory polyvinyl alcohol (PVA)/tea polyphenol (TP) hydrogels with UV shielding performance is realistically important in application fields. Herein, we designed functional PVA/TP hydrogels with excellent UV-shielding ability and improved the shape memory on hot water stimuli. This study shows that the abundant hydrogen bonds between PVA and TP are the source of shape memory. The PVA hydrogels with 8 wt% TP loading could approximately recover their original shape after deformation when immersed in water at 50 °C for 30 s. Meanwhile, the hydrogels also had excellent UV shielding capacity. After ageing under UV for 16 days, the observed shape of the hydrogel with 8 wt% TP loading retained 74.7% of the original, and the hydrogel could effectively protect the skin of mice from damage under 10 mW cm^{-2} UV irradiation. With the understanding of the UV-shielding behavior of hydrogels, this study has been able to generate biomedical materials for human skin protection, specifically skin covering the joint areas, where shape memory of the applied materials is essential.

Received 11th July 2020
Accepted 1st September 2020

DOI: 10.1039/d0ra06053d

rsc.li/rsc-advances

Introduction

Shape-memory materials have attracted substantial international research attention because of their unique performance.[1,2] Shape-memory hydrogel is an important part of shape-memory materials, and they have applications in various fields, such as soft robotics, sensors, intelligent medical devices, or implants for minimally invasive surgery.[1–9] Based on the structure-response mechanism, shape-memory hydrogels can be divided into two types of molecular interactions: supramolecular interactions and dynamic covalent bonds.[2,10] In terms of the response to external stimuli, they can be divided into temperature, chemical, pH, light and magnetic stimulus-responsive types.[11–17] Among these, temperature-responsive shape memory hydrogels belong to supramolecular interaction response mechanism,[18–20] which has been developed and applied in many high value-added fields, such as smart medical devices.[21]

Polyvinyl alcohol (PVA) hydrogel is non-toxic,[22,23] biocompatible[24,25] and one of the commonly used temperature-responsive hydrogels. As we know, a hydrogel with excellent shape-memory capacity is necessary to obtain some degree of crosslinking.[8] However, the common PVA hydrogel is not enough as shape memory material although lot of hydrogen bonds can be formed between the molecular chains. Therefore, almost no shape memory capacity is observed in the PVA hydrogel.[26] In recent years, increasing the intermolecular hydrogen bonds has been used as a strategy to improve the response speed of shape-memory PVA hydrogels through the introduction of compounds, which can form hydrogen bonds with PVA.[27–30] Li *et al.* used melamine (MA) as a physical cross-linker to form hydrogen bonds with PVA, and the physical cross-links made the composite hydrogels capable of restoring within 5 min under the therapeutic ultrasound conditions.[31] Yang *et al.* prepared a PVA composite hydrogel containing physically cross-linked networks by adding polydopamine (PDA) particles.[32] The hydrogel exhibited near-infrared light-triggered shape memory and could be recovered from a temporary shape within 180 s. Chen *et al.* reported a PVA shape-memory hydrogel that was formed mainly through the hydrogen bonds between PVA and tannic acid, which acted as strong physical cross-linking points. The hydrogel samples with a deformed shape could recover to their original shapes when immersed in water at 60 °C in few seconds.[26] In addition, sometimes, chemical crosslinking has also been introduced for increasing the shape-memory capacity.[33,34]

[a]*College of Chemistry, Chemical Engineering and Materials Science, Soochow University, Suzhou, Jiangsu, 215123, People's Republic of China. E-mail: dailixing@suda.edu.cn; qinchuanxiang@suda.edu.cn; zqq88263268@just.edu.cn*

[b]*College of Material Science & Engineering, Jiangsu University of Science and Technology, Zhenjiang, Jiangsu, 212003, People's Republic of China*

† Electronic supplementary information (ESI) available. See DOI: 10.1039/d0ra06053d

Apparently, the recovery process of most doped PVA hydrogels is relatively slow. Meanwhile, the doped substances and the chemical crosslinking process involved in the preparation of the hydrogels may introduce toxic substances, which may result in the toxicity of hydrogels, damage human health, and lead to poor biocompatibility of the hydrogels. Therefore, the application of shape-memory materials is greatly limited in the biomedical field. So far, there has been no report on rapid-response non-toxic hydrogel materials with certain medical functions.

Ultraviolet (UV) radiation is harmful to the human body,[35,36] and so, hydrogels with UV-shielding capacity have great potential for applications in corresponding environments. Recently, a few hydrogels with UV-shielding capacity were successfully prepared and produced a marked effect on the protection of skin.[37–39] For example, Lu *et al.* prepared an anti-UV conductive-polymer hydrogel by the *in situ* formation of polydopamine (PDA)-doped polypyrrole (PPy). The hydrogel could effectively protect the surface of mouse skin under strong UV radiation of 30 mW cm^{-2}.[40] Ghorbanzadeh *et al.* prepared a microemulsion-based hydrogel containing sesame oil.[41] Due to its unique chemical and physiological properties, sesame oil is a suitable candidate for the UV-protection of the skin. It is conceivable that shape-memory hydrogels with anti-UV properties will have special applications in the protection and treatment of skin. Tea polyphenols (TP) is a kind of tea-derived polyphenol containing α-benzopyran, fused aromatic hydrocarbons and polyhydroxy structures.[42] They have the advantages of non-toxicity, biocompatibility, and health-care function. When used as a dopant, TPs can form hydrogen bonds and cross-link with the matrix polymer through their hydroxyl groups (–OH) and the related groups on the polymer, and this is expected to improve the shape memory behaviour. Meanwhile, TPs have a strong UV absorption peak at 270–280 nm and superior UV resistance.[43,44] So far, TPs have not been reported as additives in shape-memory materials and their applications in UV resistance or shielding.

Herein, dual-functional hydrogels with outstanding shape memory and UV resistance properties were prepared by adding natural non-toxic TPs into PVA. A freezing-thawing method was used to form the fast-recovering shape-memory hydrogels with excellent UV resistance. The mechanical properties, UV resistance and shielding, and shape-memory property of the hydrogels were investigated. These composite shape memory hydrogels with UV shielding have good application prospects in the fields of biomedical engineering and smart sensors.

Experimental methods

Materials

PVA (alcoholysis: 97.0–98.8%; degree of polymerization: 2600) and MA (chemically pure) were purchased from China Pharmaceutical Chemical Reagents Co., Ltd. (Shanghai, China); TP (purity 98%) was purchased from Yuanye Bio-Technology Co., Ltd and used without further treatment.

Preparation of PVA/TP hydrogels

A certain amount of TP was added in deionized water, and the aqueous TP solution was treated under ultrasound for 30 min, after which a certain amount of PVA was added. After dissolving it at 90 °C for 2 h with stirring, the mixture was made to stand for 2 h at 90 °C to remove bubbles. Poly-tetrafluoroethylene (PTFE) mould had been regulated to be level, and heated for 1 h at 60 °C. Then, the uniform solution was poured into a PTFE mould. After that, according to the literature,[45] the mould containing the solution was transferred to a cooling chamber equipped with a cryogenic cooling liquid-circulating pump and frozen for 10 h at −40 °C, and then, thawed for 2 h at 25 °C to obtain the PVA/TP hydrogels with the TP loadings of 2, 4, 6, 8, and 10 wt%. For comparison, PVA/MA hydrogels were prepared as described in the literature.[31]

The water content of the prepared hydrogels was calculated as follows:

$$\text{Water content}(\%) = (m_{\text{wet}} - m_{\text{dry}})/m_{\text{wet}} \times 100\%$$

where m_{wet} and m_{dry} are the masses of the as-prepared hydrogels and the hydrogels vacuum-dried for 24 h at low temperatures to avoid destroying their structure, respectively.

Shape-memory behavior

The hydrogel strips (75 mm × 4 mm × 2 mm) were deformed by wrapping on a glass rod. The deformed hydrogels were kept at room temperature for 3 h. The shape recovery process of the deformed hydrogels was conducted by immersing them in water at 50 °C and recording them with a digital camera. On the other hand, the original straight hydrogel strips (180°) were bent to U-shape and kept for 3 h at room temperature. Afterwards, the U-shape hydrogels were put into water at 30 °C, 50 °C and 70 °C. The observed shape recovery rate (R_o) and net recovery rate (R_n) are defined as:

$$R_o = \Theta_t/180 \times 100\% \quad (1)$$

$$R_n = (\Theta_{30} - \Theta_0)/180 \times 100\% \quad (2)$$

where Θ_t, Θ_{30} and Θ_0 are the angles of the hydrogel strips after recovering for t s, 30 s and 0 s, respectively, in water at the set temperature. The recovery time t for R_n was selected as 30 s because, at this time, one of the samples (TP loading 8 wt%) nearly recovered to the original state.

Anti-UV properties

UV aging resistance. PVA/TP hydrogels with different contents of TP and the PVA/MA hydrogel were exposed to UV light (1 mW cm^{-2}) for 4, 8, 12 and 16 days, respectively. During this period, the hydrogels were sealed to avoid moisture volatilization. Then, the hydrogel samples were bent into U-shape and maintained at room temperature for 3 h. And then, the hydrogels were put into water at 50 °C to recover. The shape-recovery rates were calculated according to eqn (1) and (2).

UV-shielding capacity. The back skin of two mice (6–8 weeks) was depilated, cleaned, and then covered by a 10 × 10 × 1 mm PVA hydrogel sheet and a PVA/TP hydrogel sheet with 8 wt% TP loading, respectively. After irradiation by a UV light (10 mW cm^{-2}) for 10 min, the back skins were observed, photos were

captured using a digital camera, and then, the mice were euthanized by cervical dislocation. The skins were collected and soaked in formalin overnight. After embedding in paraffin, serial sections and HE staining were performed to observe the changes in the epidermal cell tissue under a microscope (Nikon ECLIPSE 90i fully automatic scientific research-level microscope). This investigation conformed to the Guide for the Care and Use of Laboratory Animals published by the US National Institutes of Health (NIH Publication, 8th Edition, 2011). All experimental protocols were approved by the Animal Use Subcommittee at Soochow University, China.

Characterization

X-ray diffraction analysis was performed using the X'Pert-Pro MPD diffractometer (Panalytical, Holland) with Cu-K alpha radiation under a voltage of 40 kV. The vacuum-dried hydrogels were scanned over the diffraction angle range of $2\theta = 5$–60°, with a step length of 0.026°. The ATR-FTIR spectra were obtained using a VERTEX80 Brook transform infrared instrument (Brook, Instrument, Germany) with a resolution of 4 cm^{-1} in the spectral region of 600–4000 cm^{-1}. The thermogravimetric analysis (TGA) was carried out using a Discovery thermogravimetric analyzer (TGA) (TA Instruments Inc., USA) from 40 to 600 °C at a linear heating rate of 10 °C min^{-1} under nitrogen flow (10 mL min^{-1}). The DSC curves were determined using a TA Q200 thermal analyser (TA Instruments Inc., USA) from 40 to 240 °C at a linear heating rate of 10 °C min^{-1} under nitrogen flow (10 mL min^{-1}). The UV-visible absorption spectra were measured using a TU-1900 dual-beam UV-visible spectrophotometer (Varian, Germany) from 200 to 800 nm. The morphology of hydrogels after freeze-drying was recorded by an S-4700 scanning electron microscope (Hitachi, Japan). The UV-visible transmission spectra of the samples were measured by a UV 3600-visible spectrophotometer (Shimadzu, Japan) from 200 to 800 nm. The tensile measurements were carried out on an Instron 5965 universal testing machine (Instron, USA) using a 50 N force sensor by uniaxial tension. The dumbbell hydrogel splines (total length: 75 mm, width 12.5 mm, internal width: 4 mm, thickness: 2 mm) were stretched at a speed of 10 mm min^{-1}. The dynamic mechanical analysis was carried out on square specimens (5 mm × 5 mm × 2 mm) in the shear mode using a Q800 dynamic mechanical analyzer (DMA) (TA Instrument, USA) equipped with a shear fixture. The temperature range was 25–75 °C at a strain amplitude of 15 μm and a fixed frequency of 1 Hz with a heating rate of 3 °C min^{-1}. Finally, the storage moduli (G'), loss moduli (G''), and loss factors (tan δ) were calculated using the DMA software.

Results and discussion

PVA/TP hydrogels with shape memory and UV resistance were prepared, as illustrated in Fig. 1a. The PVA and TP aqueous solutions were mixed sufficiently to become a uniform solution. Subsequently, the PVA/TP solution was cast on a PTFE mould by the classic freezing-thawing method to obtain a dumbbell-shaped shape-memory hydrogel strip. The formation of the hydrogels was caused by the network composed of PVA, TP and the hydrogen bonds between them, as shown in Fig. 1b. The mixed PVA/TP aqueous solutions with the different TP loadings are shown in Fig. 1c. With an increase in TP loading, the colour of the solutions deepened, and when the TP loading was more than 8 wt%, there was non-uniformity, when in fact the solution partly changed into a hydrogel at room temperature (25 °C), indicating that the addition of TP is good for the formation of PVA/TP hydrogels. Fig. 1d shows the SEM image of the hydrogel after freeze-drying; the microstructure of the hydrogel is a three-dimensional porous network, which is believed to be conducive to high extension and to promote rapid recovery of the hydrogel from deformation.

The water content of the hydrogel gradually decreased with increasing TP content (Fig. S1†), whereas the actual water content of the hydrogel was slightly lower than the theoretical water content. For example, the water content of the hydrogel prepared with 14 wt% PVA and 10 wt% TP should be 76 wt%, but it actually was 53.6 wt%. The loss of water is caused possibly by squeezing due to the formation of a dense cross-linked network between TP and PVA and by volatilization during the preparation process.

In order to prove the formation of hydrogen bonds between PVA and TP, ATR-FTIR characterization of the PVA, TP and PVA/TP hydrogels was performed. The absorption peaks at 3293 cm^{-1} and 3211 cm^{-1} in the spectra of PVA and TP could be attributed to –OH group stretching vibration, respectively. With an increase in TP loading in the PVA/TP hydrogels, the absorption peak shifted from 3290 cm^{-1} (2 wt% TP) to 3243 cm^{-1} (10 wt% TP). Meanwhile, the intensity of the peak at 1690 cm^{-1} designated to the C=O stretching vibration increased with increasing TP loading. This suggested the presence of hydrogen bonds between –OH on the PVA molecular chains and –OH on TP, and the number of hydrogen bonds increased with an increase in TP content,[46,47] which preliminarily illustrated that the PVA/TP hydrogels formed stronger H-bonding. Since PVA is a semi-crystalline polymer, the use of the freezing-thawing method for preparing the PVA hydrogel results in microcrystalline PVA, which plays the role of providing crosslinking points. As shown in Fig. 2b, pure PVA has distinct characteristic peaks at $2\theta = 20.3^\circ$, 22.9° and 40.2°, corresponding to the crystal planes (101), (200) and (102), respectively. The diffraction peak intensity of the PVA/TP gel at $2\theta = 20.3^\circ$ rapidly decreased from 4837 a.u. (0 wt% TP) to 825 a.u. (10 wt% TP) (Fig. S2a†). The trend of the full width at half maxima (FWHM) of the PVA/TP gels at $2\theta = 20.3^\circ$ was similar to that of the diffraction peak intensity and decreased from 0.92 (0 wt% TP) to 0.86 (10 wt% TP) (Fig. S2b†). It seemed that with an increase in the TP content of the hydrogels, the formation of microcrystalline PVA molecules was prevented, but the crystallite size increased, indicating that more polymer chains were present in each PVA crystallite.[47,48] On the other hand, there was almost no change in the position of the peaks, which meant that the lattice distance in the samples did not undergo an obvious change.[29,46]

As shown in Fig. 2c, the glass transition temperature (T_g) of the PVA/TP gel substantially increased from 79 °C (0 wt% TP) to 117 °C (10 wt% TP), which is likely because the increase in

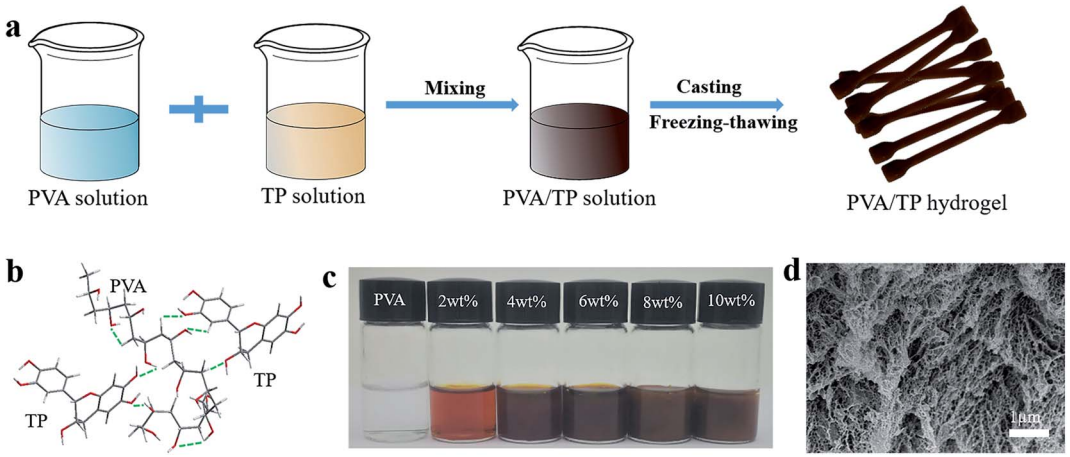

Fig. 1 (a) Preparation process of PVA/TP hydrogels. (b) Structures of the hydrogen bonds between PVA and TP. (c) Photo images of the PVA/TP composites at 25 °C. (d) SEM image of the freeze-dried PVA/TP hydrogel (8 wt% TP).

crosslinking hinders the movement of the molecular segments during the heating process, resulting in an increase in T_g. Meanwhile, the melting point (T_m) decreased with increasing TP loading, and particularly, when the content of TP was over 8 wt%, T_m disappeared, indicating that further formation of microcrystalline PVA molecules was prevented, which agrees with the XRD pattern. This further illustrated that the crystallization of the PVA/TP hydrogel decreased with increasing TP content. Fig. 2d shows the DSC diagram of the cooling crystallization of the hydrogels; like T_m, the crystallization temperatures (T_c) significantly decreased with increasing TP loading, suggesting that the crosslinking network was dense and hydrogel formed swiftly, resulting in the decrease in the crystallization capacity. Besides, as shown in Fig. S3a,† the weight loss between 0 °C and 270 °C was attributed to the evaporation of unbound and bound water in the hydrogels, while the weight loss between 300 °C and 420 °C was related with the damage of crosslinking between PVA and TP because the weight loss rate obviously decreased with TP content (Fig. S3b†). With an increase in TP content, more cross-links are formed, and so, the PVA/TP gels are difficult to decompose compared to pure PVA.

Furthermore, as shown in Fig. 2e, at TP loadings lower than 8 wt%, the stress, strain and elastic modulus of the hydrogels increased dramatically with the TP content. In addition, the stress and elastic modulus of the hydrogels showed a narrow error range (Fig. S4a and b†). When the content of TP was increased to 10 wt%, the stress of the hydrogel rose to 13.82 MPa, but the strain decreased, which was ascribed to cross-linking. Although the stress (8.75 MPa) of the hydrogel with 8 wt% TP loading was not the highest, the strain reached

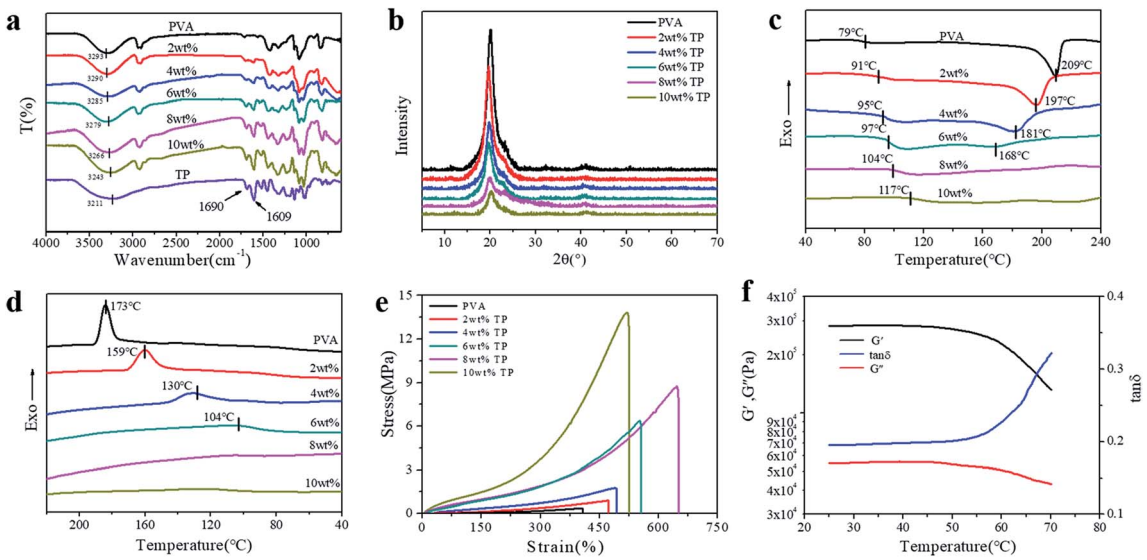

Fig. 2 (a) ATR-FTIR spectra, (b) X-ray diffraction (XRD) patterns, the (c) heating and (d) cooling DSC curves, and (e) tensile stress–strain curves of the PVA/TP hydrogels with different TP loadings. (f) Storage moduli (G′), loss moduli (G″), and loss factor (tan δ) of the PVA/TP hydrogel (8 wt% TP) as a function of temperature.

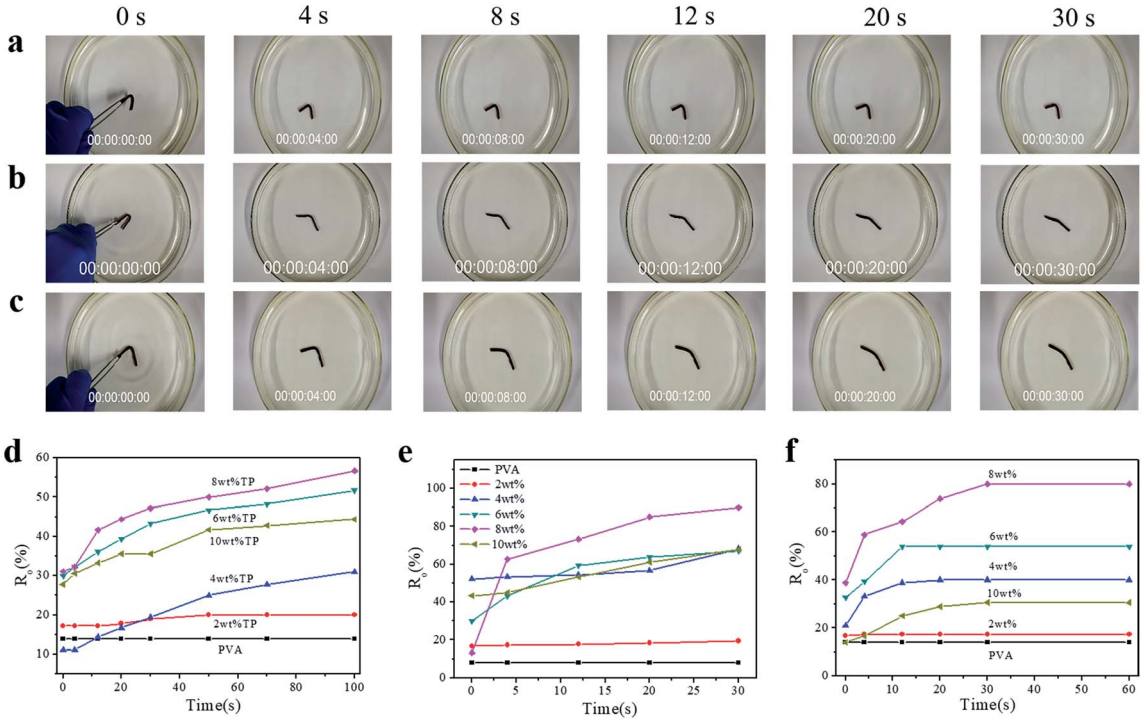

Fig. 3 Photos showing the shape-memory behavior of a PVA/TP hydrogel (8 wt%) after being immersed in water at (a) 30 °C, (b) 50 °C and (c) 70 °C for at different time points. The observed shape recovery rates (R_o) of the PVA/TP hydrogels with different TP loadings as a function of the time of immersion in water at (d) 30 °C, (e) 50 °C and (f) 70 °C.

650%, which was the highest among all the hydrogels. The stress and strain of all the PVA/TP hydrogels were higher than those of pure PVA hydrogel, and the tensile strengths of hydrogels with high TP loadings were basically higher than those with low TP loadings. In addition, the tensile strength increased with a decrease in water content (Fig. S1†). We also measured the temperature dependence of the dynamic mechanical properties of the PVA/TP hydrogels (8 wt%). As shown in Fig. 2f, when the temperature was less than 50 °C, the G′ and G″ values were mainly maintained, whereas when the temperature exceeded 50 °C, under the dual action of temperature and force, the decrease in G′ and G″ led to a sharp increase in the tan δ curve, which could be caused by the damage of the cross-links formed by weak hydrogen bonds. When the temperature reached over 70 °C, the curve changed dramatically for most of the hydrogel cross-linking networks were destroyed (Fig. S4c†). Similarly, the PVA/TP solutions with TP loadings more than 8 wt% changed into partially gelated composites at room temperature, while the composites formed uniform dark brown solutions at 70 °C (Fig. S5†).

To illustrate the shape-memory properties of the hydrogels at different temperatures, deformation was achieved by fixing the hydrogel into a U-shape and standing it at room temperature for 3 h, and then the deformed hydrogels were put in water at 30 °C, 50 °C, and 70 °C, respectively, to obtain the shape-memory properties, which were calculated according to the deformed angle (Fig. S6†). The shape-memory behavior of the PVA/TP composite hydrogels with different TP loadings at 50 °C is shown in Fig. S7,† and it is clear that the shape memory of the hydrogel with 8 wt% TP loading was the best (Fig. S7e†). Fig. 3a–c show the photos of the shape-memory recovery process of the hydrogel with 8 wt% TP at 30 °C, 50 °C and 70 °C, respectively. The recovery was the lowest at 30 °C, the fastest at 50 °C and medium at 70 °C. At 30 °C, the energy provided is not enough to damage the cross-links, while at 70 °C, part of the original cross-linking and the temporary cross-links formed between weak hydrogen bonds and microcrystallites are damaged. Fig. 3d–f show the R_o of the hydrogels with different TP contents at different temperatures. The R_o values of pure PVA hydrogel formed nearly a straight line, while the R_o of the PVA/TP hydrogels increased with an increase in TP content except for the hydrogel with the TP loading 10 wt%. The R_o and R_n of the hydrogel with 8 wt% TP content were higher than those of the other PVA/TP hydrogels (Fig. S8†), and R_o and R_n reached the maximum of 90% and 76.7% at 50 °C, respectively. When the content of TP was further increased to 10 wt%, the hydrogel showed a particularly low R_o value, perhaps because the temporary cross-linking system was too stable to be destroyed.

Besides the U-shape memory, we fixed the hydrogel strips around a glass rod and kept it for 3 h at room temperature to form spring-like hydrogels. Then, we put the deformed hydrogels into hot water at 50 °C to observe the recovery process, as shown in Fig. 4a and S9.† After 48 s in hot water, the hydrogel could restore its shape without rings when the TP loading was 8 wt%, and the trend of shape recovery of the hydrogels with increasing content of TP was extremely similar to that of the U-shaped hydrogels. The shape-memory recovery process at the microscale is illustrated schematically in Fig. 4b. As shown in

Fig. 4b, in the original hydrogel, strong physical cross-linking points are formed by hydrogen bonding between –OH on TP and –OH on the PVA chains, in addition to the hydrogen bonds between the PVA chains, through the freezing-thawing process. When the hydrogel is fixed to a specific shape, a small part of the hydrogen bonds restructure to adapt to the external stress. Meanwhile, under strain, the hydrogel is subjected to deformation of chain orientation that results in the formation of temporary crosslinking between the microdomains of the crystallized PVA chains and weak hydrogen bonds. When the hydrogel is exposed to hot water after the removal of the external force, the PVA molecular chains and TP molecules begin to relax, the temporary crosslinking is disrupted, and the structure of the hydrogel returns to the original state. Therefore, once the external force is released, the original shape is restored or partially restored under the external stimulus, *e.g.* hot water.

This process was confirmed by the ATR-FTIR spectra and DSC curves of the PVA/TP gels. As shown in Fig. 4c, the stretching vibration peak of –OH in the original state was at 3266 cm^{-1}, while it shifted to the high wavenumber 3283 cm^{-1} for the deformed shape, indicating the decrease in hydrogen bonds. After recovery, the –OH stretching peak shifted to 3269 cm^{-1}, which is similar to that of the original state. As shown in Fig. 4d, the original state of the PVA/TP gel had a T_g of 104 °C, and no melting peak was seen for the crystallites. After deformation, the T_g of the PVA/TP gel decreased to 99 °C, and a new melting peak at 164 °C appeared, whereas after recovery, T_g increased to 105 °C, which is close to that of the original state, and the melting peak disappeared. Evidently, when the shape of the hydrogel was restored, the microstructure was restored as well.

As stated above, shape-memory hydrogels have the potential to be applied extensively, even in environments with continuous UV irradiation. Fig. 5a–d show R_o of the PVA/TP hydrogels irradiated or aged continuously for 4–16 days under UV light. With an increase in TP content in the hydrogels, R_o increased with the recovery time after immersion in water at 50 °C for the hydrogels with different aging time. Particularly, R_o of the hydrogel with 8 wt% TP loading at 30 s was still higher than those of the other hydrogels with different TP contents. After 16 days of aging, R_o and R_n of the hydrogel with 8 wt% TP loading were 67.2% and 52.2%, accounting for 74.7% and 68.1% of the values of the hydrogel without irradiation, respectively (Fig. S10†). A schematic diagram of the shape recovery of the hydrogel with 8 wt% TP loading after 16 days under UV irradiation and without UV irradiation is illustrated in Fig. 5e, and the recovery angle of the former at 30 s and 50 °C water reached about 70% of the latter, indicating excellent UV resistance. As shown in Fig. 5f, the –OH stretching peak of the PVA/TP gel with 8 wt% TP loading without UV irradiation shifted from 3266 cm^{-1} to a higher wavenumber of 3302 cm^{-1} for the PVA/TP gel after 16 days of UV aging. Thus, long-term UV aging results in the partial breakage of hydrogen bonds even when TP is added although the hydrogel has satisfactory UV resistance.

In order to further confirm UV resistance, the shape-memory PVA/MA hydrogel was prepared, and its resistance to UV irradiation was investigated. R_o and R_n of the original PVA/MA hydrogel were 47.2% and 32.8%, respectively, while after 16 days irradiation, they decreased to 8.3% and 2.3%, respectively (Fig. S11†). The UV resistance was far lower than that of the PVA/TP hydrogel with 8 wt% TP loading.

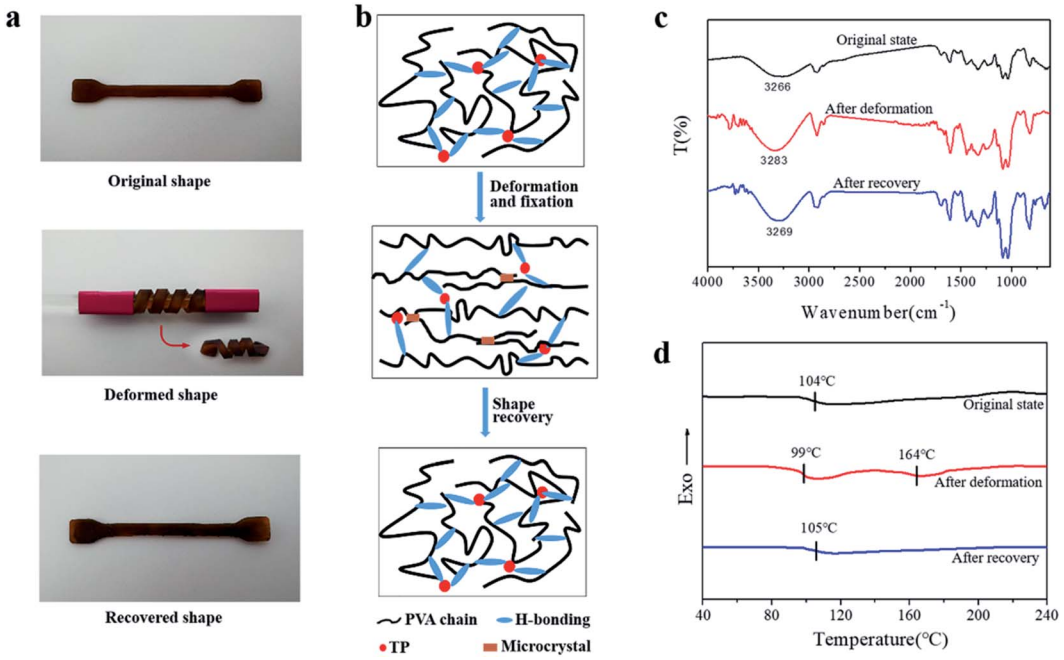

Fig. 4 (a) Photos showing the shape-memory behavior of a PVA/TP hydrogel strip (8 wt% TP); (b) temperature-responsive shape memory mechanism of the PVA/TP hydrogel; (c) the ATR-FTIR spectra and (d) heating DSC curves of the PVA/TP hydrogel (8 wt% TP) in the original, deformed and recovered states.

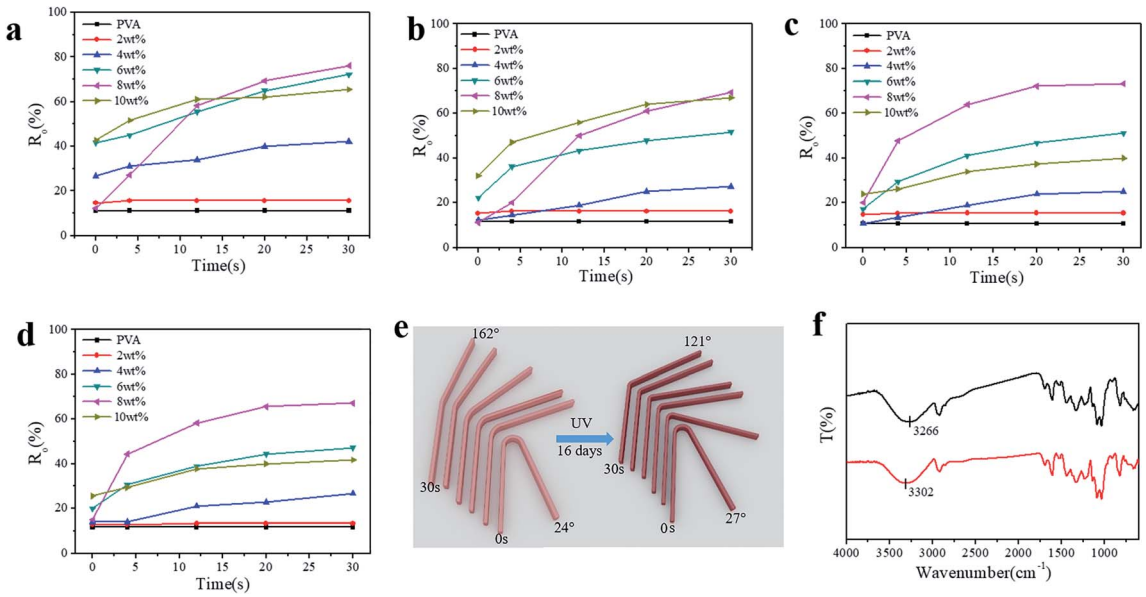

Fig. 5 Observed Shape recovery rates (R_o) of the PVA/TP hydrogels with different TP loadings as a function of UV aging time: (a) 4, (b) 8, (c) 12 and (d) 16 days, (e) schematic diagram of the shape recovery of the hydrogel with 8 wt% TP loading with and without UV irradiation, and (f) ATR-FTIR spectra of the PVA/TP hydrogel (8 wt% TP) after 16 days of UV irradiation (above) and without UV irradiation (below).

As shown in Fig. S12a and b,† the UV absorption spectra of solutions with different TP contents in water showed strong characteristic absorption peaks at 274 nm due to the aromatic group in TP, and the UV absorbance of the TP solution increased with increasing TP content. This shows that the PVA/TP hydrogel may play a significant role in absorbing the ultraviolet light even with a small amount of TP (Fig. S12c†). When the TP content was increased to 10 wt%, UV light could not pass

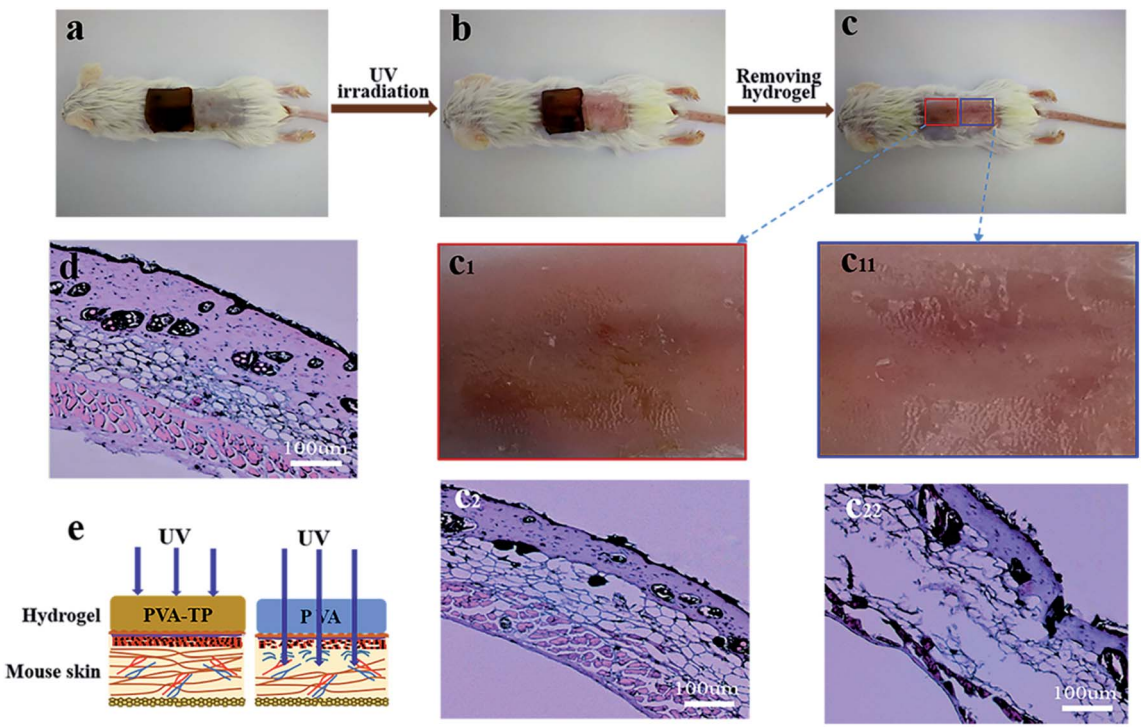

Fig. 6 Photos of the hydrogels covering the back skin of a rat (a) without UV radiation and (b) with UV irradiation; (c) photo of the UV-irradiated mouse back skin after removing the PVA/TP and PVA hydrogels. Magnified photos of the mouse back skin covered by (c_1) the PVA/TP and (c_{11}) PVA hydrogels after UV irradiation. H&E staining of the skin tissue protected by (c_2) the PVA/TP hydrogel and (c_{22}) the PVA hydrogel. (d) H&E staining of the skin tissue without UV irradiation, and (e) schematic demonstration of UV shielding by the hydrogels used as skin dressing.

through the hydrogel. As shown in Fig. 6a–c, the square sheets of PVA and the PVA/TP hydrogel with 8 wt% TP loading were used to cover different portions of mouse skin and irradiated under a strong UV source. The skin surface covered by the composite hydrogel was not harmed by the UV irradiation (Fig. 6c1), while the skin covered by the PVA hydrogel was seriously injured (Fig. $6c_{11}$). Further, the adipose tissue and muscle fibroblasts in the epidermis of mice skin covered by the PVA/TP hydrogel remained intact (Fig. $6c_2$) and was comparable with the skin morphology without UV irradiation (Fig. 6d). In contrast, skin covered by the PVA hydrogel showed significant injury with ruptured collagen fibers, as illustrated in Fig. 6c22, which proved that the composite hydrogel has excellent UV-shielding property and can protect the skin, as schematically illustrated in Fig. 6e.

Conclusions

In summary, a dual-functional PVA/TP hydrogel was designed and prepared with improved stimuli-response speed for shape memory and excellent UV-shielding property through the introduction of UV-resistant and multi-hydroxyl-containing TP into PVA. The microstructural changes in the deformation process of the PVA/TP shape-memory hydrogel were studied in detail, and it was evident that the temporary shapes were determined by both the microdomains of the crystallized PVA chains and the weak hydrogen bonds, for the first time. The PVA/TP hydrogels showed remarkable hot water stimulus-response behavior, and R_o of the hydrogel with 8 wt% TP loading reached up to 90% after recovery for 30 s. More importantly, the PVA/TP hydrogels exhibited outstanding UV resistance. After the hydrogel with 8 wt% TP loading was aged under UV for 16 days, its R_o was 74.7% of the original, and on the other hand, the hydrogel sheet could almost completely protect the skin of mice from damage under 10 mW cm^{-2} UV irradiation, showing excellent UV-shielding capacity. Thus, the novel dual-functional PVA/TP hydrogels demonstrated momentous potential in many exciting applications, such as wound dressing, UV-shielding body covers, and intelligent medical devices.

Conflicts of interest

There are no conflicts to declare.

Acknowledgements

This research is supported by National Key Research and Development Program of China (2017YFB0309401), a Project Funded by the Priority Academic Program Development of Jiangsu Higher Education Institutions.

Notes and references

1 T. Xie, *Polymer*, 2011, **52**, 4985–5000.
2 A. Lendlein and S. Kelch, *Angew. Chem., Int. Ed.*, 2002, **41**, 2034–2057.
3 A. Lendlein, H. Jiang, O. Jünger and R. Langer, *Nature*, 2005, **434**, 879.
4 W. Guo, C. H. Lu, R. Orbach, F. Wang, X. J. Qi, A. Cecconello, D. Seliktar and I. Willner, *Adv. Mater.*, 2015, **27**, 73–78.
5 G. Li, G. Fei, H. Xia, J. Han and Y. Zhao, *J. Mater. Chem.*, 2012, **22**, 7692–7696.
6 M. C. Serrano, L. Carbajal and G. A. Ameer, *Adv. Mater.*, 2011, **23**, 2211–2215.
7 X. Li and M. J. Serpe, *Adv. Funct. Mater.*, 2016, **26**, 3282–3290.
8 W. Lu, X. Le, J. Zhang, Y. Huang and T. Chen, *Chem. Soc. Rev.*, 2017, **46**, 1284–1294.
9 H. Zhang, D. Han, Q. Yan, D. Fortin, H. Xia and Y. Zhao, *J. Mater. Chem. A*, 2014, **2**, 13373–13379.
10 W. Wei, Y. Zhang and W. Liu, *Prog. Polym. Sci.*, 2017, **71**, 1–25.
11 J. R. Kumpfer and S. J. Rowan, *J. Am. Chem. Soc.*, 2011, **133**, 12866–12874.
12 X. Tao, *Nature*, 2010, **464**, 267–270.
13 R. H. Xie, P. G. Ren, H. Jian, R. Fang, L. Z. Ren and Z. F. Sun, *Carbohydr. Polym.*, 2016, **138**, 222–228.
14 B. Hua, L. Chun, W. Xiaolin and S. Gaoquan, *Chem. Commun.*, 2010, **46**, 2376–2378.
15 X. Le, W. Lu, H. Xiao, L. Wang, C. Ma, J. Zhang, Y. Huang and T. Chen, *ACS Appl. Mater. Interfaces*, 2017, **9**, 9038–9044.
16 M. Kohei, N. Masaki, T. Yoshinori and H. Akira, *Angew. Chem., Int. Ed.*, 2015, **54**, 8984–8987.
17 D. Zhen-Qiang, C. Ya, Y. Qi-Juan, W. Yi-Fu, L. Jian-Hu, L. Bang-Jing and Z. Sheng, *Macromol. Rapid Commun.*, 2013, **34**, 867–872.
18 C. Xu, Q. Tang, H. Yang, K. Peng and X. Zhang, *Macromol. Chem. Phys.*, 2018, **219**, 1700636–1700642.
19 J. Hao and R. Weiss, *ACS Macro Lett.*, 2013, **2**, 86–89.
20 F. Chen, K. Yang, D. Zhao and H. Yang, *RSC Adv.*, 2019, **9**, 18619–18626.
21 R. Z. Alavijeh, P. Shokrollahi and J. Barzin, *J. Mater. Chem. B*, 2017, **5**, 2302–2314.
22 S. Azmi, S. I. A. Razak, M. R. Abdul Kadir, N. Iqbal, R. Hassan, N. H. M. Nayan, A. H. Abdul Wahab and S. Shaharuddin, *Soft Mater.*, 2017, **15**, 45–54.
23 M. Kobayashi, Y. S. Chang and M. Oka, *Biomaterials*, 2005, **26**, 3243–3248.
24 W. K. Wan, G. Campbell, Z. F. Zhang, A. J. Hui and D. R. Boughner, *J. Biomed. Mater. Res.*, 2002, **63**, 854–861.
25 M. Kobayashi and H. S. Hyu, *Materials*, 2010, **3**, 2753–2771.
26 Y. N. Chen, L. Peng, T. Liu, Y. Wang, S. Shi and H. Wang, *ACS Appl. Mater. Interfaces*, 2016, **8**, 27199–27206.
27 Z. Lu, Z. Wang, X. Chen, L. Yi and L. Yu, *J. Mater. Chem.*, 2011, **21**, 10399–10406.
28 L. Guo, Z. Hongji, F. Daniel, X. Hesheng and Z. Yue, *Langmuir*, 2015, **31**, 11709–11716.
29 W. Zhao, C. Gao, H. Sang, J. Xu, C. Wang and Y. Wu, *RSC Adv.*, 2016, **6**, 52982–52986.
30 T. Liu, C. Jiao, X. Peng, Y. N. Chen, Y. Chen, C. He, R. Liu and H. Wang, *J. Mater. Chem. B*, 2018, **48**, 8105–8114.
31 G. Li, Q. Yan, H. Xia and Y. Zhao, *ACS Appl. Mater. Interfaces*, 2015, **7**, 12067–12073.

32 L. Yang, Z. Wang, G. Fei and H. Xia, *Macromol. Rapid Commun.*, 2017, **38**, 1700421.
33 T. Hirai, H. Maruyama and T. Suzuki, *J. Appl. Polym. Sci.*, 1992, **45**, 1849–1855.
34 H. Meng, J. Zheng, X. Wen, Z. Cai, J. Zhang and T. Chen, *Macromol. Rapid Commun.*, 2015, **36**, 533–537.
35 M. Claire, T. Caroline and B. Françoise, *Int. J. Mol. Sci.*, 2014, **16**, 68–90.
36 F. Afaq and H. Mukhtar, *J. Photochem. Photobiol., B*, 2001, **63**, 61–69.
37 A. Svobodovã, J. Psotovã and D. Walterovã, *Biomed. Pap.*, 2003, **147**, 137–145.
38 L. A. Balestrin, J. Bidone, R. C. Bortolin, K. Moresco, J. C. Moreira and H. F. Teixeira, *J. Photochem. Photobiol., B*, 2016, **163**, 269–276.
39 A. Dey, R. Bera, S. Ahmed and D. Chakrabarty, *J. Ind. Eng. Chem.*, 2015, **21**, 1219–1230.
40 H. Lu, L. Yan, M. Wang, K. Wang and L. Xiong, *Chem. Mater.*, 2018, **30**, 5561–5572.
41 M. Ghorbanzadeh, N. Farhadian, S. Golmohammadzadeh, M. Karimi and M. Ebrahimi, *Colloids Surf., B*, 2019, **179**, 393–404.
42 C. S. Robb, S. E. Geldart, J. A. Seelenbinder and P. R. Brown, *J. Liq. Chromatogr. Relat. Technol.*, 2002, **25**, 787–801.
43 W. Wen-Bin, C. Han-Sun, F. Jia-You, C. Shao-Kuan, H. Chieh-Chen and H. Chi-Feng, *Life Sci.*, 2006, **79**, 801–807.
44 K. Rajesh and G. B. Maru, *Food Chem.*, 2006, **94**, 331–340.
45 F. Yokoyama, I. Masada, K. Shimamura, T. Ikawa and K. Monobe, *Colloid Polym. Sci.*, 1986, **264**, 595–601.
46 X. Qi, X. Yao, S. Deng, T. Zhou and Q. Fu, *J. Mater. Chem. A*, 2014, **2**, 2240–2249.
47 Y. Huang, M. Zhang and W. Ruan, *J. Mater. Chem. A*, 2014, **2**, 10508–10515.
48 X. Hong, C. Xiong, G. Jia, L. Jianbin, A. Matthew, I. Stephan and J. Donglin, *Chem. Commun.*, 2014, **50**, 1292–1294.